ACS ES&T Air

Open Access

pubs.acs.org/estair

Article

TROPOMI Satellite Data Reshape NO_2 Air Pollution Land-Use Regression Modeling Capabilities in the United States

M. Omar Nawaz,* Daniel L. Goldberg, Gaige H. Kerr, and Susan C. Anenberg

Cite This: *ACS EST Air* 2025, 2, 187−200

Read Online

ACCESS | Metrics & More | Article Recommendations | Supporting Information

ABSTRACT: Nitrogen dioxide (NO_2) pollution is associated with adverse health effects, but its spatial variability between ground monitors is poorly characterized. NO_2 column observations from the Tropospheric Monitoring Instrument (TROPOMI) have unprecedented spatial resolution and high accuracy over the globe. Land-use regression (LUR) models predict surface-level NO_2 with relevance for epidemiological and environmental justice studies. We use TROPOMI NO_2 columns in a land use regression (LUR) model to improve surface NO_2 concentration estimates over the United States. The TROPOMI LUR predictions have improved correlation with ground monitors (Adj. R^2 = 0.72) and bias (Mean Bias, MB = 14.2%) compared with an existing LUR using less granular NO_2 data from a legacy satellite instrument (Adj. R^2 = 0.54 and MB = 49%; for North America). Removing TROPOMI NO_2 from the LUR decreased R^2 by 29.1%, 8.1 times the impact of removing road system information. These findings reveal that novel Earth observing satellites can enhance surface NO_2 surveillance by capturing pollution variation between monitors without relying heavily on other data sources.

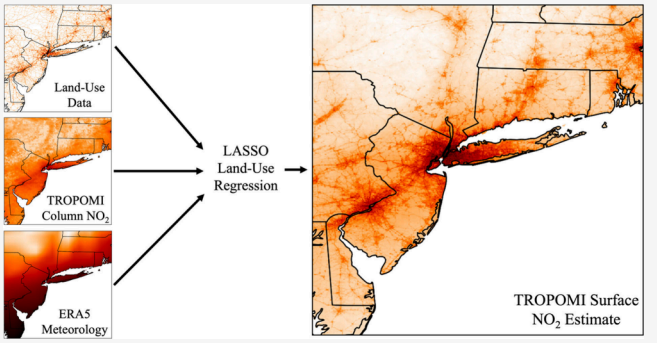

KEYWORDS: *air quality, pollution, health, environmental justice, nitrogen dioxide, statistical modeling*

1. INTRODUCTION

Nitrogen dioxide (NO_2) is an air pollutant that is emitted during fossil-fuel combustion[1] and is associated with adverse health effects.[2−6] The short atmospheric lifetime of NO_2[7] leads to spatial heterogeneity in its surface-level concentrations due to its 5−8 h daytime lifetime.[8,9] Statistical models that predict surface-level NO_2 generally assume that NO_2 is strongly associated with land-use characteristics linked to its emission—as examples, road systems and built-environment—given this short atmospheric lifetime.[10] These statistical land-use regression (LUR) models balance the influence of predictor variables like land-use characteristics and remote-sensing observations of atmospheric column NO_2 and use ground-level observations to develop predictions of surface-level concentrations at fine spatial resolution and with wide spatial coverage that are needed for many types of studies. For example, epidemiological and risk assessment studies characterize the relationship between NO_2 exposure and adverse health effects—such as pediatric asthma incidence[6] and cardiovascular mortality.[11] These studies require fine-scale ($\leq$1 km) estimates of NO_2 to accurately capture the colocation of peaks in concentration with high population density to avoid underestimating health effects.[12] Additionally, environmental justice studies that investigate the spatial distribution of air pollution to determine if marginalized groups bear a disproportionate share of pollution[13,14] require data inputs that capture neighborhood-scale variability in concentration patterns. Prior LUR models have featured the use of numerous land-use characteristics simultaneously; however, this approach has potential disadvantages. For example, these LUR models may pick up on patterns in combinations of land-use variables that are correlated with NO_2 concentrations but that predict unrealistic patterns in surface-level concentrations. New satellite-based remote-sensing observations at finer spatial resolution may enable the development of LURs that depend on fewer land-use variables while still maintaining or improving upon the statistical performance of older models; however, this has not yet been tested.

In recent years, satellite remote-sensing instruments have improved our understanding of the spatial distribution of column NO_2.[15,16] Diurnal patterns,[17] vertical mixing,[18] horizontal advection,[19] boundary-layer heights,[20] and chemical interactions[8] lead to differences between column and surface-level NO_2 that can complicate the conversion of columns to surface-level concentrations. To account for this, both

Received: July 4, 2024
Revised: January 7, 2025
Accepted: January 8, 2025
Published: January 22, 2025

deterministic modeling[21,22] and statistical modeling[23,24] approaches have been developed to infer surface-level NO_2 concentrations from remote-sensing column observations. These approaches have used remote-sensing observations from different instruments. The TROPOspheric Monitoring Instrument (TROPOMI) observes atmospheric slant columns of NO_2 globally—once per day at approximately 13:30 local time (LT)—at a resolution of 5.5 × 3.5 km^2.[25] These slant columns are converted to vertical columns using an air mass factor[26] and—given the variable day-to-day observation angle of TROPOMI—these vertical columns can be spatially averaged through oversampling to capture spatial variability in column values at fine resolution (e.g., 1 × 1 km^2) at the expense of the temporal resolution.[16] The spatial resolution of TROPOMI is improved compared to its predecessor—the Ozone Monitoring Instrument (OMI)—that observes slant columns of NO_2 at a much coarser resolution of 24 × 13 km^2.[27] Roughly 16 TROPOMI pixels are contained in a single OMI pixel. On the other hand, OMI has a greater temporal coverage (October 2004 to present) than TROPOMI (April 2018 to present).

TROPOMI data have been used extensively in statistical models to estimate surface-level NO_2 concentrations. These data have been used in kriging,[28] machine-learning,[29,30] and land-use regression[31] models for predicting NO_2 in East Asia and similar techniques have been applied for California[32,33] and in Europe.[34] Other studies have combined these satellite remote sensing data with chemical transport model simulations to predict surface-level NO_2 globally,[22] in Europe,[35−37] and in East Asia.[38] Global LUR models that have incorporated OMI data[23,24] have had a high dependence on land-use characteristics in their predictions. To date, no study has investigated how the enhanced spatial resolution from TROPOMI could affect the influence of land-use characteristic predictor variables—in comparison to satellite remote-sensing observations—on LUR predictions. Additionally, the effect of TROPOMI observations on LUR performance compared to older OMI-derived models remains poorly understood.

In this study, we explore how the inclusion of oversampled remote-sensing observations from TROPOMI at fine spatial resolution (1 × 1 km^2) impacts LUR modeling. To investigate this, we develop a TROPOMI-derived LUR (TROPOMI-LUR) model to predict monthly average surface-level NO_2 concentrations from 2019 to 2022 across the CONUS. This TROPOMI-LUR is trained with ground-level observations of monthly averaged NO_2 concentrations from the US Environmental Protection Agency (EPA) Air Quality System (AQS) from 516 instruments across 48 months for a total of 20394 observations after filtering. This TROPOMI-LUR is built using predictor variables from three distinct categories: land-use characteristics, TROPOMI satellite remote-sensing observations of NO_2 columns, and meteorological reanalysis data. To explore how TROPOMI data impact LUR modeling we formulate two specific research questions that we investigate through application of the TROPOMI-LUR: first, will the inclusion of high spatial resolution oversampled TROPOMI observations improve the predictive accuracy of the LUR compared to an older OMI-derived LUR (OMI-LUR)[24] and second, second, how is the comparative influence of land-use characteristics and remote-sensing observations affected by the inclusion of TROPOMI observations? Through addressing these two questions, we aim to characterize how TROPOMI data affect the prediction of surface-level NO_2 and determine if any improvements are associated with an increased emphasis on TROPOMI data in place of land-use characteristics. These fine-resolution estimates can enable the broader community to better understand recent NO_2 trends, conduct quantitative risk assessments, and assess inequities in population exposure and health impacts attributable to NO_2.

2. MATERIALS AND METHODS

2.1. Experimental Design. In this study we design a land-use regression (LUR) model informed by TROPOMI observations to 1) identify if including high spatial resolution oversampled satellite observations improves the predictive accuracy of LUR modeling of surface-level NO_2 compared to older products, and 2) determine how influential land-use characteristics are compared to satellite remote-sensing observations on LUR predictions to identify if satellite data from TROPOMI can simplify future modeling. To achieve these objectives, we download and process observations of surface-level NO_2 from the US EPA AQS, download and oversample TROPOMI observations of column NO_2, download other LUR predictor variables such as road systems, built environment, and elevation, perform feature selection on these predictor variables, build our LUR model, and carry-out cross-validation statistical testing.

2.2. Ground-Level Observations of NO_2. We obtain hourly observations of surface-level NO_2 from 516 unique instruments located throughout the CONUS from 2019 to 2022 for the purpose of training the TROPOMI-derived LUR model; these hourly data are downloaded from the US EPA AQS Web site (https://aqs.epa.gov/aqsweb/airdata/download_files.html: accessed Jan 28th, 2024). We follow the averaging approach used in a previous study[24] to calculate monthly averaged surface-level NO_2: we average data based on local time and remove daily observations from monitors with less than 18 h and monthly observations from monitors with less than 50% of days in a month. We further filter these data by removing any monthly averaged observations that are unrealistically high (above 200 ppb). Given that some locations have multiple unique instruments, we perform these averaging and filtering steps for each instrument and each site. A majority of the EPA AQS monitors measure NO_2 using chemiluminescence instruments that have demonstrated a consistent high bias[27] due to the counting of other reactive nitrogen species as NO_2; this bias is seasonally dependent and higher in rural sites compared to urban; we do not correct for this bias so that our predicted model is comparable to the OMI-LUR and because many past epidemiological studies have derived statistical relationships between health effects and this uncorrected NO_2. We weight monitor values when building the LUR based on a formula from a prior study.[23]

We investigate patterns in the distribution of surface-level NO_2 using observations from the EPA AQS to identify potential deficiencies in our predictive model that could arise due to data sparsity. Understanding over- and under-represented characteristics of monitors in our training data set is necessary to qualitatively characterize where our LUR model is most applicable and where there is more uncertainty; features that are not captured or underrepresented in the training data set will consequently not be well represented in LUR predictions. Similarly, features that are overrepresented in the training data set may appear in LUR predictions even if they are unrealistic. Given that a focus of our analysis is to determine the comparative influence of specific predictor

https://doi.org/10.1021/acsestair.4c00153
ACS EST Air 2025, 2, 187−200

variables (i.e., land-use characteristics compared to remote-sensing observations), it is especially relevant to consider features of the ground-level monitors used in our training data set that could influence predicted patterns in surface-level NO_2. We examine the features of our training data set by mapping the distribution of ground-level monitors across the CONUS for 2019 (Figure 1a) and consider seasonal (Figure 1b) and interannual (Figure 1c) patterns across four of the largest metropolitan areas in the US. Additionally, we calculate summary statistics of the monthly average (Table S1) and annual (Table S2) observation overall and for specific years, seasons, and monitor characteristics (i.e., near-road and urban classifications).

Throughout our analysis and model building we consider specific monitor characteristics to identify unique patterns in observations and predictions associated with specific seasons, years, and monitor types. We identify the observation as being in one of four seasons—December, January, February (DJF), March, April, May (MAM), June, July, August (JJA), and September, October, November (SON) based on the month the measurement was taken. We also identify the observations by the year that they occurred in between 2019 and 2022. Lastly, we identify two additional characteristics of monitors, whether they are "near-road" and if they are "urban" or "rural". Near-road monitors—those that are within 50 m of a major highway feature—are tracked by the US EPA;[39] all monitors that are not "near-road" are denoted as "non-road", however, we note that these "non-road" monitors can still be near smaller roads and/or slightly outside of the 50 m buffer defined by the US EPA. We identify urbanicity using global built-up data from GHS-SMOD[40] following previous methods;[5,41,42] this data set identifies urban boundaries by considering grid cell contiguity, population density per grid cell, and total population across the extent. Monitors that are located within one of the cities identified in the US using these data are considered "urban" and monitors that are not located in any one of these cities are considered "rural".

2.3. Oversampled TROPOMI NO_2 Columns. We obtain publicly available daily observations of column NO_2 from the TROPOMI instrument on board the Sentinel-5 Precursor satellite (https://data-portal.s5p-pal.com/products/no2.html) coincident with our model time frame (2019−2022) and spatial domain (CONUS). For this study we use L2 data from version 2.4.0 (RPRO Jan 1, 2019−July 25 2022, OFFL July 26, 2022−Dec 31, 2022) that are vertical columns derived from slant columns using the operational AMF from GEOS-CF; data with a quality assurance flag below 0.75 were discarded. The TROPOMI instrument observes column NO_2 at a native pixel size of 5.5 × 3.5 km^2 and approximately once per day at 1:30 PM and has made observations from August 2018 to present.

For this study, we further process these TROPOMI data through an oversampling that spatially averages the coarse size variable pixels of TROPOMI to a standard grid of 0.01° × 0.01° resolution—that is, approximately 1 km × 1 km—using the technique introduced by Goldberg et al. 2021.[16] Specifically, in this method we identify whether the center grid point of a 0.01° × 0.01° grid cell is within any portion of a valid TROPOMI pixel. If so, the value of the 0.01° × 0.01° degree grid cell is the value of the overlapping TROPOMI pixel for the overpass time, and then all valid observations over the month are averaged (method depicted in Figure S1). We perform this oversampling for each month of our study domain, and oversample seasonal averages for the four sets of three months described in section 3.3. During cloudier and colder months TROPOMI observations in the northern US—especially in the Great Lakes region—are sparse; in these areas the oversampled NO_2 columns can be missing or retain discontinuities associated with the TROPOMI pixel shapes. To account for this, we modify the oversampled products based on

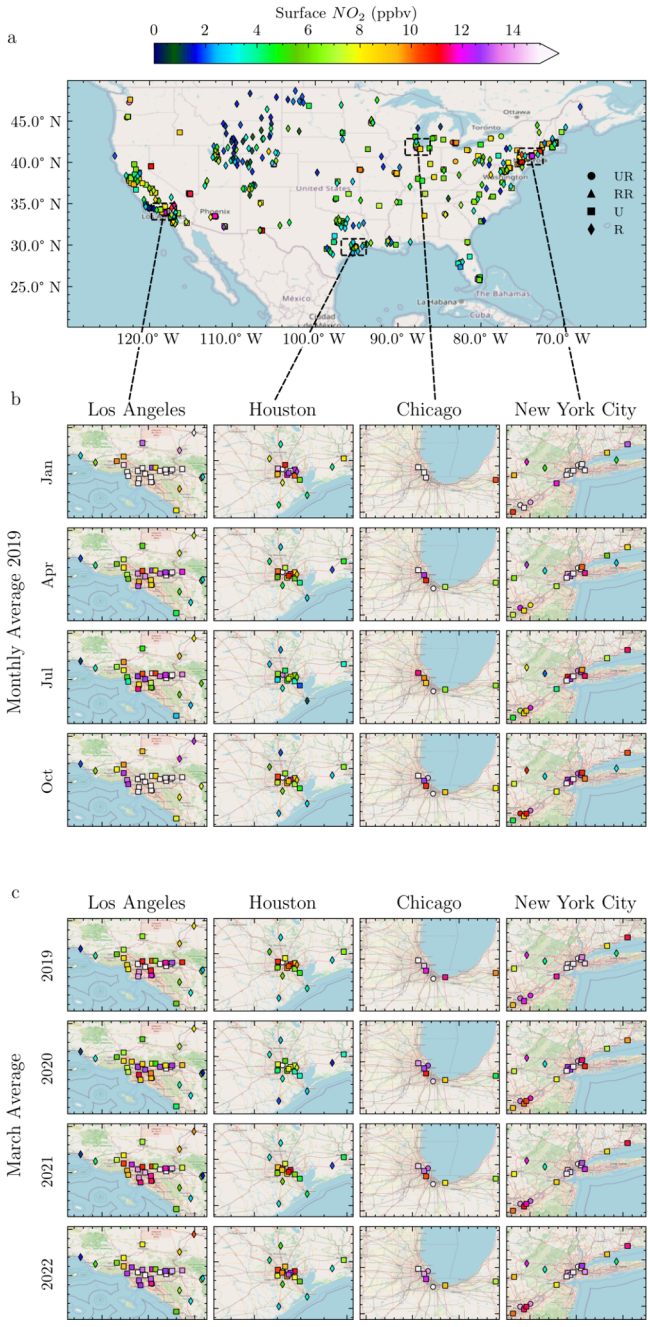

Figure 1. NO_2 concentrations observed by EPA AQS monitors, for 2019 annual average (a), 2019 monthly averages in four metropolitan areas (b), and monthly averages in March across four years for the four same metropolitan areas (c). Lines on these plots indicate major highways and primary roads. Monitor characteristics are indicated by shapes: circular points refer to near-road monitors in urban areas (UNR), triangular points refer to near-road monitors in rural areas (RNR), squares refer to monitors in urban areas that are not classified as "near-road" (U), and diamonds refer to monitors in rural areas that are not classified as "near-road" (R).

https://doi.org/10.1021/acsestair.4c00153
ACS EST Air 2025, 2, 187−200

the number of overpasses that are included in each pixel. For each month and each grid cell, if a cell has fewer than five overpasses included in the averaging then we instead use the seasonal average of the same year. If the seasonal average also has fewer than five overpasses, we replace it with the annual oversampled TROPOMI values from the same year. In doing so we ensure that oversampled data that is noisy is not included in our LUR model; however, we note that this could weaken seasonal trends, especially in the wintertime, at higher latitudes given that—for some grid cells—annual values are used instead of the monthly or seasonal values.

2.4. Other Predictor Variables Included in LUR Model.

Beyond the remote-sensing observations from TROPOMI—discussed in the prior section—we include predictor variables of two other types: characteristic of or associated with land-use data and meteorological reanalysis data from ERA-5.[43] These variables are downloaded from three sources: OpenStreetMap (OSM), Google Earth Engine, and from the European Centre for Medium-Range Weather Forecasts (ECMWF) Reanalysis Model v5 (ERA5) database.[44] We provide summary information for these predictor variables in Table 1 below:

Table 1. Basic Information for All Predictor Variables Considered in TROPOMI-Derived LUR Model[a]

Predictor Variable	Year(s)	Temporal scale	Spatial scale	Source
TROPOMI column NO_2	2019-2022	Monthly	0.01°	25
2-meter Temperature	2019-2022	Monthly	0.25°	43
Surface pressure	2019-2022	Monthly	0.25°	43
Total precipitation	2019-2022	Monthly	0.25°	43
UV backscatter	2019-2022	Monthly	0.25°	43
Water	2000	N/A	0.001°	45
Elevation difference	2000	N/A	0.001°	46
Built environment	Average 1985-2018	N/A	0.001°	47
Population density	Average 2000-2020	N/A	0.001°	48
Major roads	2019	N/A	N/A	49
Minor roads	2019	N/A	N/A	49
Residential roads	2019	N/A	N/A	49
Major rails	2019	N/A	N/A	49
Minor rails	2019	N/A	N/A	49

[a]Selected variables are shaded in grey.

OpenStreetMap is an open and editable database of geographic information; in this study we use data identifying roads and railways. We downloaded road and rail information from OSM and followed classifications established by Larkin et al. 2023[24] to differentiate "major", "minor", and "residential" roads and "major" and "minor" railways. We convert these data from vectors to raster density values by overlaying the vector data onto the 0.01° × 0.01° TROPOMI-LUR grid and then by counting the number of segments for each feature that passes through each grid cell. We note that the road data in this study is pulled for a different year (i.e., 2019) than used by Larkin et al. 2023[24] (i.e., 2018).

ERA5 is a reanalysis product that contains hourly estimates of different meteorological properties. For the TROPOMI-LUR we consider boundary layer height, 2-m temperature, total precipitation, and surface pressure that were downloaded from the ERA5 database of the monthly average 24-h average levels. These data are available at a 31 × 31 km^2 resolution and they are linearly interpolated onto the 0.01° × 0.01° grid using a bilinear interpolation to smooth out discrete boundaries between grid cells. These data—along with the TROPOMI observations—are the only time-varying predictor variables; the rest are considered static in time.

The remaining predictor variables—that is, elevation, water, built environment, and population—were downloaded from Google Earth Engine at a resolution of 0.001° × 0.001° (approximately 100 m × 100 m). These products come from different sources that are indicated in Table 1. We process the elevation data as an "elevation-differential" that considers elevation levels relative to surrounding elevation by calculating the average within a certain radius of each grid cell and differencing each grid cell based on this relative average. Specifically, we calculate the average elevation for each 1° increment and then perform a bilinear-interpolation to the 0.01° resolution; we then take the difference between these values and the native elevation values to calculate the difference relative to the nearby area. The rest of these predictor variables are not adjusted with the exception that all variables are spatially aggregated to the LUR grid of 0.01° × 0.01°.

2.5. Development of the LUR and Statistical Analysis.

At the start of the development of the TROPOMI-LUR we consider all the above predictor variables; however, we perform feature selection steps to narrow down the list of relevant predictor variables. We perform a Lasso regression[50] that has been widely used in LUR models[23,24] to identify the variables that have no impact on predictions through minimization of their coefficients; the Lasso regression adds a L1 regularization term to the linear regression model that shrinks coefficients to zero for predictor variables that do not have a strong statistical relationship to the dependent variable. The first step of feature selection is to transform the predictor variables and observations. For all the observations and all variables—except TROPOMI observations—we apply a square root transformation to the data; for TROPOMI observations we apply a natural log transformation. To avoid including noisy data from observations with low NO_2 levels from TROPOMI, we set a lower bound for TROPOMI values of 9E14 molecules cm^{-2} such that all values below this cutoff are set to a value of 9E14 molecules cm^{-2}. We do this to stabilize variances across the predictor variables and linearize relationships between these predictor variables and the observations. Additionally, we standardize the predictor variables so that they are centered around zero and so that they have comparable standard deviations.

We construct the TROPOMI-LUR by processing the land-use characteristic, remote-sensing observations, and meteorological reanalysis predictor variables (Section 2.3 and 2.4) and training the predictions using EPA AQS monitor observations of monthly surface-level NO_2 (Section 2.2 and 3.1) by applying a least absolute shrinkage and selection operator (Lasso) regression analysis (Section 2.4). The predictive accuracy of this TROPOMI-LUR model is then evaluated by performing 10,000 "leave 10% out" cross-validations in which we reserve 10% of monitor locations for testing and use the other 90% for building the TROPOMI-LUR model. In this cross-validation analysis, we evaluate the TROPOMI-LUR predictions against the 10% testing data set and calculate the average statistical performance across all 10,000 runs for the monthly predictions (Table 4) and for the annual averages of the monthly predictions (Table 5). We choose to perform a site-specific cross-validation—leaving out 10% of monitors as

https://doi.org/10.1021/acsestair.4c00153
ACS EST Air 2025, 2, 187−200

opposed to leaving out 10% of all observations—as this allows us to not only evaluate the performance of the overall TROPOMI-LUR predictions but also the performance for different years, seasons, and monitor characteristics. We calculate annual average predictions by averaging the monthly predictions from the TROPOMI-LUR; however, we also tested an annual model and found comparable performance.

After this first feature selection step, the predictor variables are further narrowed down by considering their statistical impact on predictive accuracy of the model. We remove each remaining predictor variable from the model and quantify the change in R^2 and MSE compared to the base model; predictor variables that worsened both R^2 and MSE or that did not have a notable (>0.1%) impact on either measure were removed. We identify the regularization coefficient ($\alpha = 0.0013$) through built-in cross-validation in the Lasso LUR model from the python scikit-learn package and use this model as the final statistical model.

We evaluate the performance of the Lasso LUR through 10,000 cross-validation runs in which we randomly select 10% of all instruments and reserve these as a testing data set and build the model using the other 90%. We calculate the performance statistics for each of these runs, the performance statistics for specific subcategories of monitors, and the performance statistics if each of the selected predictor variables were removed. When we present cross-validated statistics in the results section we take the mean values of the statistics across all 10,000 runs. Any subcategory that had fewer than 15 monitors in the testing data set were excluded from the average.

For each predictor variable, we compare the TROPOMI-LUR predictions against the testing data and calculate R^2 values for two cases: 1) if all predictor variables are included and 2) if the predictor variable is removed. We then calculate the extent to which the R^2 value decreased by removing the predictor variable and calculate the average reduction in R^2 value across all 10,000 cross-validations. Through this analysis, we identify how impactful each predictor variables is on the predictive accuracy of the TROPOMI-LUR and then consider the influence of these predictor variables on the TROPOMI-LUR compared to the OMI-LUR.[24]

The influence of predictor variables differs dramatically between the TROPOMI-LUR and OMI-LUR and thus we anticipate that these two models will predict distinct spatial distributions of surface-level NO_2. Additionally, we anticipate that these models will have different performance when compared to overall and subgroups of EPA AQS observations. To evaluate this, we compare the annual average predictions for 2019—the only year in which the two models overlapped—from the TROPOMI-LUR to the OMI-LUR directly to compare the spatial distributions of surface-level NO_2 predicted by these two models (Figure 4a). We then compare these predictions to annual average observations across the EPA AQS monitors in 2019 (Figure 4b and Table 3). We perform a nearest-neighbor interpolation of the coarser TROPOMI-LUR predictions to the OMI-LUR grid so that we can calculate spatial absolute and relative differences (Figure 3a); however, the performance statistics (Figure 4b and Table 3) were calculated at the native resolutions of each LUR—approximately 1×1 km^2 for the TROPOMI-LUR and 50×50 m^2 for the OMI-LUR—by identifying, for each monitor, its grid cell location.

3. RESULTS

3.1. Exploratory Analysis of Ground-Level Observations and Predictor Variables. We present patterns in the distribution of surface-level NO_2 observations from EPA AQS monitors (Figure 1) and summarize statistics of the monthly average (Table S1) and annual average (Table S2) observations overall and for specific years, seasons, and monitor characteristics (i.e., near-road and urban classifications).

Across the EPA AQS monitors, observations of monthly surface-level NO_2 from 2019 to 2022 exhibit regional, seasonal, and interannual patterns that have been previously documented.[51] The most extreme concentrations of NO_2 are located in areas of high population density including the Northeastern US and Southern California (Figure 1). These regions have among the highest density of monitors throughout the US which suggests that the TROPOMI-LUR model built from these data will exhibit features specific to these areas and predictions will be less uncertain for these regions. Notably, there are few monitors within the Central US and Northwestern US—besides in urban areas—and thus we anticipate LUR predictions will be more uncertain in these areas. We find that average NO_2 observations in the winter months of December, January, and February (DJF)—when there are more favorable photochemical conditions for NO_2 formation and persistence[52]—were 66% higher than in the summer months of June, July, and August (JJA) (Table S2) when considering observations across all four years. Additionally, there was greater variability in winter months ($\sigma^2 = 5.42$) than in summer months ($\sigma^2 = 4.14$) as expected due to the greater data spread (8% larger range). Monthly average (Table S1) and annual average (Table S2) observations did not exhibit notable interannual patterns except for a drop in mean values (−7%) from 2019 to 2020, consistent with observed decreases in NO_2 associated with lockdowns in response to the COVID-19 pandemic.[14,22,53−55]

Most of the monthly observations in our training data set fall into one of three categories: urban nonroad (N = 9057), rural nonroad (N = 8276), and urban near road (N = 2965). The "non-road" sites specifically refer to monitor locations that are not directly adjacent (within 50 m) to major roads or major road features (e.g., on-ramps); these sites may still be near less-trafficked roads and/or outside of the 50-m range near major roads. Urban near-road sites have higher mean NO_2 values (12.6 ppb) than the nonroad urban (9.1 ppb) sites due to their immediate proximity to high vehicle emissions of nitrogen oxides (NO_x). Additionally, NO_2 observations are 135% greater at the urban nonroad sites than at the rural nonroad sites; this is consistent with prior studies that find that the largest sources of NO_2 are well correlated with urbanicity.[56,57]

3.2. Evaluating the Predictive Accuracy of the TROPOMI-LUR Model. We present an evaluation of the LUR predictions using cross-validation (for methodological details see Section 2.3) to determine the performance of the monthly average surface-level NO_2 predictions (Table 2) and the annual-averages of our monthly predictions (Table 3). After evaluating the predictive accuracy of the TROPOMI-LUR at the monthly and annual time scales, we present the distribution of annual predictions from the TROPOMI-LUR for 2019 and assess its capability for capturing seasonal and interannual variability (Figure 2) and investigate interurban patterns in predicted NO_2 (Figure 3). Definitions of all

https://doi.org/10.1021/acsestair.4c00153
ACS EST Air 2025, 2, 187−200

Table 2. Mean Statistics of 10,000 "Leave 10% of Monitors out" Cross-Validation Runs That Compare TROPOMI-LUR Predictions of Monthly Surface-Level NO_2 Across the Continental United States to United States Environmental Protection Agency (EPA) Air Quality System (AQS) Observations in the 10% Testing Dataset Across All Monitors (Total) and Across Different Years, Seasons, and Monitor Types

	N	RMSE	R^2	Adj. R^2	MB (%)	NMB (%)
Year						
2019	507	2.79	0.72	0.71	10.72	−4.71
2020	518	2.52	0.74	0.74	15.46	−2.21
2021	519	2.61	0.72	0.71	16.24	−1.16
2022	516	2.62	0.72	0.72	14.18	−2.47
Season						
DJF	513	2.72	0.75	0.75	9.22	−3.66
MAM	515	2.50	0.66	0.65	15.11	−0.61
JJA	519	2.62	0.60	0.59	16.77	−1.94
SON	514	2.68	0.73	0.73	15.54	−3.47
Type						
Urban Nonroad	915	2.60	0.69	0.68	13.93	4.58
Urban Road	298	3.91	0.51	0.49	−18.53	−20.49
Rural Nonroad	838	1.87	0.54	0.54	26.72	1.89
Total	2061	2.64	0.72	0.72	14.17	−2.66

Table 3. Average Statistics of 10,000 "Leave 10% Of Monitors out" Cross-Validation in Predicting Annual Surface-Level NO_2 Across the CONUS and Across Different Years and Monitor Types as for Table 2, but Using Annual Surface-Level NO_2 Concentrations

	Number	RMSE	R^2	Adj. R^2	MB (%)	NMB (%)
Year						
2019	46	2.32	0.76	0.72	6.74	−3.80
2020	45	2.08	0.77	0.73	10.32	−1.78
2021	47	2.20	0.75	0.71	10.94	−1.10
2022	45	2.22	0.74	0.70	8.81	−2.24
Type						
Urban Nonroad	82	2.04	0.70	0.67	8.68	4.83
Urban Road	28	3.49	0.51	0.35	−18.97	−20.26
Rural Nonroad	75	1.55	0.56	0.52	20.07	2.30
Total	183	2.22	0.75	0.75	9.25	−2.25

statistics—including root-mean-square error (RMSE), Pearson R-squared (R^2), adjusted R-squared (Adj. R^2), mean percent bias (MB), and Normalized Mean Bias (NMB)—are presented in the supplement (Section S2).

The TROPOMI-LUR predictions of monthly surface-level NO_2 are well correlated with observations (R^2 = 0.72) with some unsystematic error (RMSE = 2.6 ppbv) and minimal biases (MB = 14.2% and NMB = −2.7%) (Table 2). Ultimately, across all monitors (total) the TROPOMI-LUR captures general patterns in observations without any major biases; we compare this performance to the OMI-LUR[24] in section 3.4 and primarily focus on the comparative performance across different subcategories of monitors in this section. In general, the predicted NO_2 values are well correlated (R^2 between 0.51 and 0.75) with observations regardless of the monitor subgroup (Table 2). Biases are also generally minimal (NMB between −4.7% and 4.6%) except for the urban near-road monitors where there is a large negative bias (−20.5%)

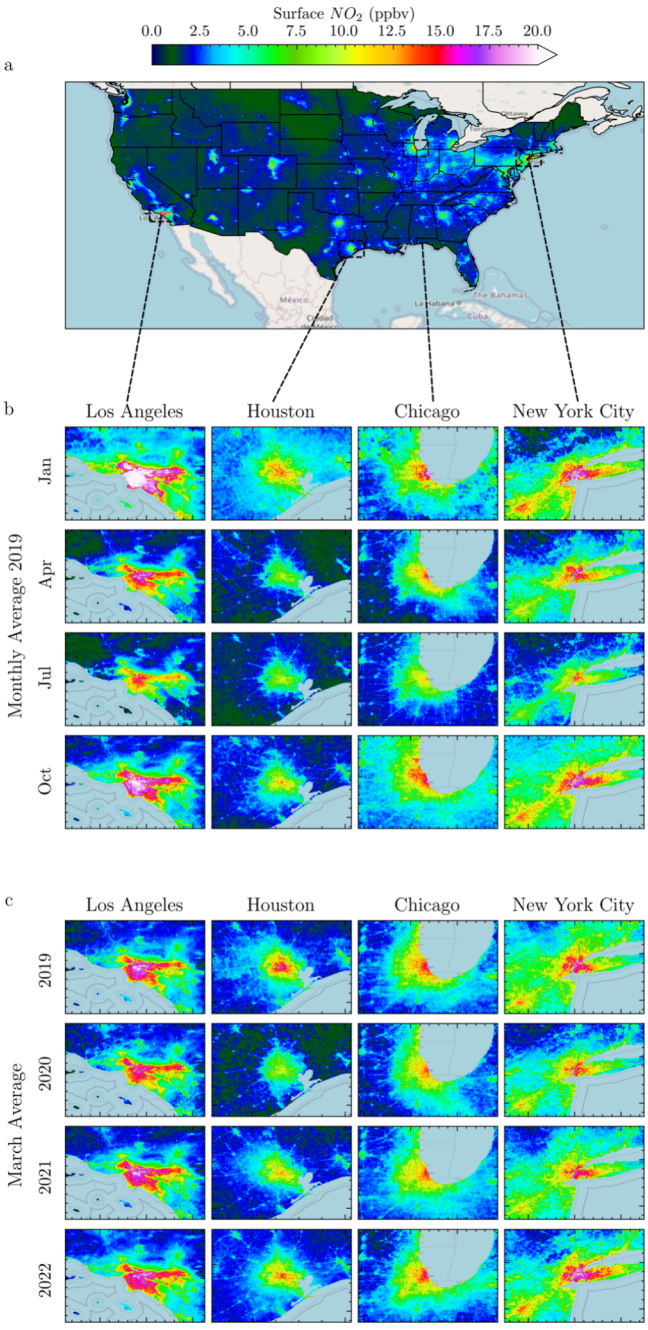

Figure 2. TROPOMI-LUR predictions of annual-average surface-level NO_2 across the CONUS for 2019 (a). TROPOMI-LUR predictions of monthly-average surface-level NO_2 January, April, July, and October 2019 across four major US metropolitan areas demonstrating monthly variability in the TROPOMI-LUR predictions (b). TROPOMI-LUR predictions of monthly-average surface-level NO_2 for March 2019−2022 for four major US metropolitan areas demonstrating annual variability in the TROPOMI-LUR predictions (c).

that is discussed in greater detail in the next paragraph. Overall, the TROPOMI-LUR model has consistently strong predictive accuracy regardless of year; however, there are greater variations in performance when considering observations across different seasons and monitor types.

The TROPOMI-LUR predictive accuracy is consistent regardless of year from 2019 to 2022: RMSE ranges between 2.5 and 2.8 ppbv, R^2 ranges between 0.72 and 0.74, and NMB

https://doi.org/10.1021/acsestair.4c00153
ACS EST Air 2025, 2, 187−200

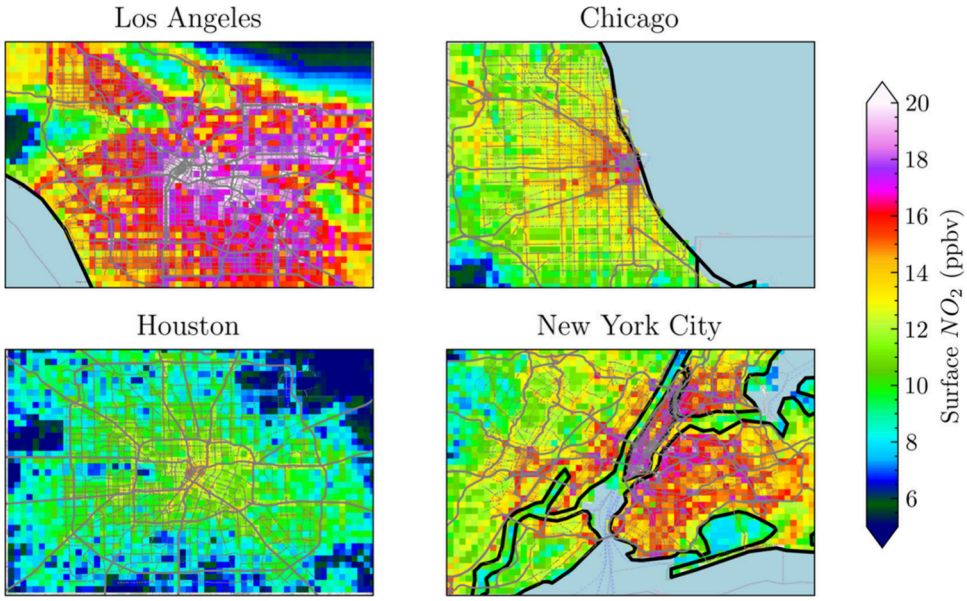

Figure 3. TROPOMI-LUR predictions of annual-average surface-level NO_2 for 2019 across the four same major urban areas compared to OpenStreetMaps road networks in gray.

% ranges between −1.2 and −4.7. There are greater variations in TROPOMI-LUR predictive accuracy when evaluating observations for different seasons. Predictions of surface-level NO_2 in the spring—March, April, and May (MAM)—and summer months are more poorly correlated (R^2 = 0.66 and 0.60, respectively) than the fall—September, October, and November (SON) and winter months (R^2 = 0.73 and 0.75, respectively). This degradation in correlation is likely attributable to lower NO_2 magnitudes in the spring and summer and is consistent with lower unsystematic errors in the spring (RMSE = 2.5 ppbv) and summer (RMSE = 2.6 ppbv) than in the fall (RMSE = 2.7 ppbv) and winter (RMSE = 2.7 ppbv). Normalized mean biases are generally consistently minimal across all four seasons; however, there is a more pronounced low-bias in the winter (NMB = −3.7%) and fall (NMB = −3.5%) than in summer (NMB = −1.9%) and spring (NMB = −0.6%). For urban nonroad monitor locations, the TROPOMI-LUR predictions have similar correlations and errors (R^2 = 0.69, RMSE = 2.6 ppbv) as predictions across all sites; however, predictions for this subgroup are slightly biased high (NMB = 4.6%). The predictions at rural nonroad monitors have worse correlation to observations (R^2 = 0.54) than other locations; however, this is likely due again to lower NO_2 magnitudes at these sites and we note that the unsystematic error is lower at these locations than across any other subgroup (RMSE = 1.9 ppbv). Observations at rural nonroad monitors are biased positive (NMB = 1.9%) indicating that the TROPOMI-LUR slightly overpredicts concentrations for these rural nonroad monitors. The LUR predictions are generally well-correlated with observations from near-road monitors with some unsystematic error at (R^2 = 0.51; RMSE = 3.9 ppbv); however, predictions for near-road locations have a notable low bias (NMB = −20.5%).

Next, we evaluate the predictive accuracy of the annual average surface-level NO_2 predictions that are calculated by taking the annual average of the monthly TROPOMI-LUR predictions of surface-level NO_2. Overall, we find that the TROPOMI-LUR annual averages agree well with annual average observations from the EPA AQS monitors. Across all locations, the annual-average predictions from the TROPOMI-LUR (Table 3) are improved (R^2 = 0.75; RMSE = 2.2 ppbv; MB% = 9.3; NMB% = −2.3) compared to monthly LUR (Table 2) predictions (R^2 = 0.72; RMSE = 2.6 ppbv; MB% = 14.2; NMB% = −2.7), albeit slightly. The adjusted Pearson correlation coefficient squared (Adj. R^2) values were lower—especially for the urban road locations—due to the limited number of observations nearing the number of predictor variables. This is a current limitation of our evaluation method that is attributable to the low number of annual observations which are restricted by the shorter record of TROPOMI observations, as more years of data become available the adjusted R^2 values should approach the R^2 values. To avoid evaluating cross-validations with very few samples, we only calculated the averages for cross-validations in which there was a minimum of 15 observations in the testing data set for each subcategory.

The TROPOMI-LUR model predicts surface-level NO_2 patterns that are consistent with the spatial and temporal patterns of the EPA AQS observations (Figure S2 and S3) as well as similar patterns to the distribution of population density (Figure S4). Specifically, the TROPOMI LUR captures wintertime peaks and summertime lows as exhibited by the EPA AQS observations and there is no apparent seasonal pattern in the differences between LUR predictions and AQS observations (Figure S5). For 2019, the TROPOMI-LUR predicts the colocation of peaks in surface-level NO_2 and high population density (Figure 2a); these areas of high population generally have a greater density of sources of NO_x (e.g., elevated vehicle traffic and industrial emissions). In general, there are higher levels of NO_2 in the Eastern US than in the Western US outside of major urban areas such as Los Angeles, San Francisco, Portland, and Seattle. In background areas, the TROPOMI-LUR predicts only minor variations in surface-level NO_2 compared to other areas. When we zoom into the four cities and consider predicted annual surface-level NO_2 for 2019, (Figure 3) we find that the spatial distribution of concentrations captures some elements of built environment and road networks; however, gradients in concentration are

https://doi.org/10.1021/acsestair.4c00153
ACS EST Air 2025, 2, 187−200

generally gradual as informed by the oversampled TROPOMI NO_2 column observations.

Considering the monthly predictions across the four major urban areas in 2019 (Figure 2b)—Los Angeles, Houston, Chicago, and New York City—we find that the TROPOMI-LUR predictions capture seasonal patterns that are consistent with what was found in the EPA AQS observations. Specifically, there are elevated concentrations of NO_2 in colder months (e.g., January) than in warmer months (e.g., July) that is attributable to lower rates of photolysis in the wintertime. The TROPOMI-LUR predictions also capture expected patterns in interannual variability when we compare predictions across the month of March for the four years (Figure 2c). We note that the model captures the decrease of NO_2 during the COVID-19 pandemic (Figure S3). Many process-based models struggled to capture the pronounced decreases during 2020−2021 (e.g., Kerr et al., 2022);[58] incorporating TROPOMI NO_2 measurements in our model allows us to avoid relying on NO_x emissions inventories, which are exceedingly difficult to update in near-real time to reflect natural changes in air quality like those induced by behavioral changes related to COVID-19.

3.3. Influence of Predictor Variables on TROPOMI-LUR Predictive Accuracy. We next evaluate how the inclusion of the high spatial resolution remote-sensing observations from TROPOMI influence the predictive accuracy of the TROPOMI-LUR. In this section we compare the influence of the predictor variables for our TROPOMI-LUR to the older OMI-LUR;[24] however, we emphasize that these two data sets have different characteristics, respectively: monthly vs daily temporal resolution, CONUS vs global coverage, and 0.1° × 0.1° vs 50 m × 50 m resolution. Thus, differences in predictor variable influence are not solely driven by the choice of remote-sensing data (i.e., TROPOMI vs OMI) but also these other distinctive characteristics.

In the TROPOMI-LUR, the influence of remote-sensing observations supplanted that of land-use characteristics—the most influential predictor variable in the global OMI-LUR[24]—making TROPOMI column NO_2 the dominant predictor variable. Removing remote-sensing observations from the TROPOMI-LUR led to a 29.1% reduction in R^2 values which was by the far the most influential predictor variable. Comparatively, removing remote-sensing observations from the global OMI-LUR only led to a 6.2% reduction in R^2 values. We note that the OMI-LUR was also evaluated for the maximum reduction in R^2 values across all regions and by this metric the % reduction in R^2 was higher −15.2%—but, since it is unclear which of the regions this reduction corresponded to, we only compare to the global statistics for the OMI-LUR in Table 4.

For the TROPOMI-LUR, built environment and major roads were the only land-use characteristics which had a notable impact on R^2 values when they were removed (−3.6% and −3.3% respectively). Meteorological properties including surface pressure (−2.4%), UV backscatter (−1.9%), and 2-m temperature (−0.6%) had a comparable influence on LUR predictive accuracy as the land-use characteristics. These results differ dramatically from the OMI-LUR in which land-use characteristics including major roads (−8.6%), built environment (−1.6%), population density (−1.5%), tree cover (−1.1%), and residential roads (−0.8%) had the greatest influence on the model. Remote-sensing observations from OMI (−6.2%) had less than half as much influence on R^2 values when they were removed from the global model than the land-use characteristics. Meteorological properties such as temperature (−0.5%) and surface pressure (−0.1%) had little influence on the OMI-LUR predictive accuracy. Overall, this evaluation suggests that remote-sensing observations are the major contributor to the statistical performance of the TROPOMI-LUR whereas the statistical performance of the OMI-LUR was more dependent on a combination of land-use characteristics and remote-sensing observations with minimal influence from meteorological properties.

Table 4. Average Influence of Each Predictor Variable on R^2 Across 10,000 Cross-Validations for the Monthly TROPOMI-Derived LUR at 0.1° × 0.1° (TROPOMI-LUR) (This Study) and the Global Daily OMI-Derived LUR (OMI-LUR) at 50 m × 50 m from Larkin et al. 2023 and LUR Model Characteristics

	% Reduction in R^2	
Predictor Variable	TROPOMI LUR	OMI LUR
Satellite Remote Sensing	29.1	6.2
All Major Road	3.6	8.6
Built Environment	3.3	1.6
Surface Pressure	2.4	0.1
UV Backscatter	1.9	N/A
Temperature	0.6	0.5
Population Density	N/A	1.5
Tree Cover	N/A	1.1
All Residential Road	N/A	0.8
Water Body	N/A	0.7
Characteristics		
Time scale	Monthly	Daily
Spatial Coverage	CONUS	Global
Spatial Scale	0.01°	50 m

3.4. Comparison between TROPOMI-LUR and OMI-LUR Predictions of Surface-Level NO_2 in 2019. We compare the predictions of surface-level NO_2 from the TROPOMI-LUR (this study) to the OMI-LUR[24] directly (Figure 4; top) and then evaluate the predictions from these two models against US EPA AQS monitor observations (Figure 4; bottom) for the only year in which there were overlapping predictions—2019.

Patterns in the spatial distribution of the TROPOMI-LUR are distinct from the OMI-LUR and they highlight the influence of different predictor variables (Figure 4a). Both models capture peaks in the urban cores of the four cities—Los Angeles, Houston, Chicago, and New York City—however, the OMI-LUR predicts sharp gradients around road-systems that are not predicted in the TROPOMI-LUR. Gradients in surface-level NO_2 are more diffuse in the latter product within the urban core; however, they generally drop to lower background levels more sharply than the OMI-LUR. Overall, the OMI-LUR predicts higher values of surface-level NO_2 in 2019 throughout much of the domain especially near road systems.

We next evaluate the predictions of surface-level NO_2 in 2019 across 458 monitors and consider the performance across specific subgroups of monitors (Figure 4 and Table 5). We find that, generally, the TROPOMI-LUR predictions of surface-level NO_2 agree better with observations than the OMI-LUR predictions. Across all locations, the TROPOMI-derived LUR has improved correlation (R^2 = 0.76) and bias (MB = 6.4%) compared to the OMI-derived LUR (R^2 = 0.70 and MB =

https://doi.org/10.1021/acsestair.4c00153
ACS EST Air 2025, 2, 187−200

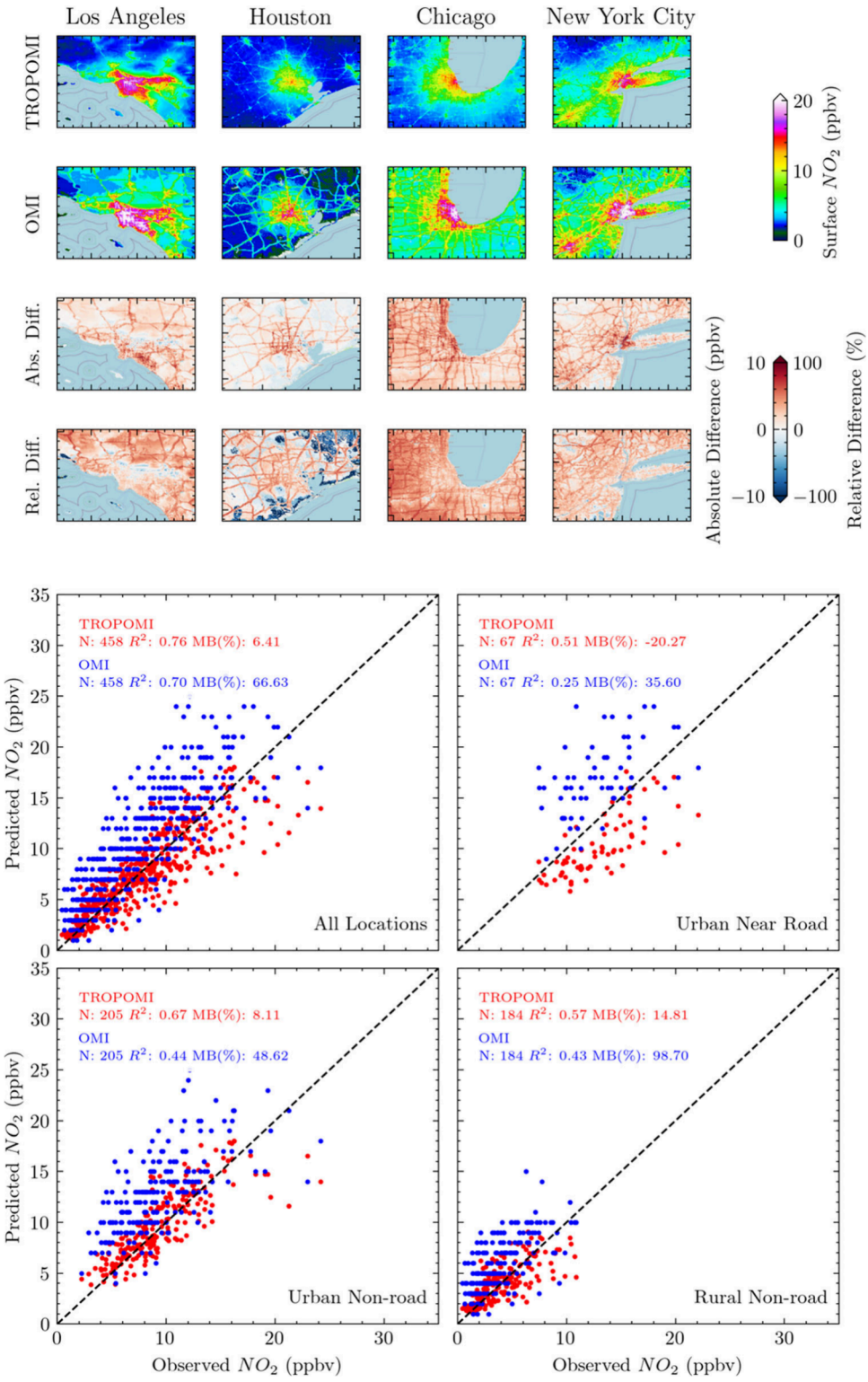

Figure 4. Annual average predicted surface NO_2 concentrations across four major urban areas for LURs using remote sensing observations from TROPOMI and OMI, and their absolute and relative differences (OMI − TROPOMI) (top). Comparisons of the predicted NO_2 from TROPOMI-LUR (red) and OMI-LUR (blue) compared to annual averaged EPA AQS surface-level NO_2 observations in 2019 across all locations, at the urban near-road, urban nonroad, and rural nonroad monitors (bottom).

66.6%) indicating that the TROPOMI-LUR predicts values that are more likely to explain variance in observations without bias. Given that remote-sensing observations from TROPOMI were responsible for substantial improvements in R^2 (Section 3.3), it is likely that this statistical improvement is at least partially attributable to the inclusion of these TROPOMI data in place of OMI data.

We also consider the performance of the two LUR models across different subgroups of monitors. Considering the monitors that are not located within 50 m of a major road

https://doi.org/10.1021/acsestair.4c00153
ACS EST Air 2025, 2, 187−200

Table 5. Statistical Performance of the TROPOMI-Derived LUR and OMI-Derived LUR Predictions of Annual Average Surface-Level NO_2 Across All Monitors and Different Subgroups of Monitors in 2019

	N	RMSE	R^2	MB (%)	NMB (%)
TROPOMI LUR					
All	458	2.32	0.76	6.41	−3.84
Urban Nonroad	205	2.22	0.67	8.11	3.44
Urban Road	67	3.73	0.51	−20.27	−21.39
Rural Nonroad	184	1.55	0.57	14.81	−0.14
OMI LUR					
All	458	4.23	0.70	66.63	39.17
Urban Nonroad	205	4.72	0.44	48.62	37.39
Urban Road	67	5.40	0.25	35.60	30.44
Rural Nonroad	184	3.01	0.43	98.70	56.32

system first, for these "urban non-road" sites, the TROPOMI-LUR (R^2 = 0.67 and MB = 8.1%) outperforms the OMI-LUR (R^2 = 0.44 and MB = 48.6%). Additionally, at the rural nonroad sites, there is improved performance in the predictions of the TROPOMI-LUR (R^2 = 0.57 and MB = 14.8%) compared to the OMI-LUR (R^2 = 0.43 and MB = 98.7%). Lastly, we note that the TROPOMI-LUR has enhanced predictive performance for near-road monitor locations than the OMI-LUR despite its much coarser (1 × 1 km^2) resolution (compared to 50 × 50 m^2). For these sites, the TROPOMI-LUR was better correlated with a more minimal error and bias (R^2 = 0.51, RMSE = 3.73 ppbv, and MB = −20.3%) compared to the OMI-LUR (R^2 = 0.25, RMSE = 5.4 ppbv, and MB = 35.6%).

We note that these statistics are not cross-validated (see Tables 2 and 3 for cross-validated statistics from this study) and that these are based exclusively on the final LUR models for the TROPOMI-LUR and OMI-LUR, respectively. Given that the monitors used to build these models are included in the evaluation statistics for Figure 4b and Table 5, these statistics should only be considered in a comparative sense between the two LUR models and should not be used to evaluate the model accuracy. To evaluate the TROPOMI-LUR model accuracy the cross-validated statistics in section 3.2 should be used instead.

To further investigate how the inclusion of TROPOMI data affects the model capabilities compared to OMI, we developed a LUR prediction in which we include annual oversampled data from OMI for 2021 in place of TROPOMI and compared it to the original TROPOMI-LUR predictions (Figure S6). In this sensitivity analysis, we generally find decreased correlation and increased biases when replacing TROPOMI observations with OMI observations especially for near-road and rural locations.

4. DISCUSSION

Given the greater reliance on satellite remote-sensing observations and less dependence on land-use data, we anticipate that the predictions of the TROPOMI-LUR—that was developed in this study—will be more representative of areas not near surface-monitors and that patterns in these predictions will more accurately represent surface-level NO_2. This data set is especially relevant for research in assessing exposure, health impact, and equity in recent years following the COVID-19 pandemic. The monthly and annual TROPOMI-LUR surface NO_2 estimates are freely available as a public good via Zenodo as version V1.01 (accessible at: https://doi.org/10.5281/zenodo.14646033). As TROPOMI continues to collect observations of column NO_2 these add to the record of remote-sensing observations that in turn can be included in building LUR models; we intend to maintain and update the TROPOMI-LUR with the availability of new remote-sensing observations and ground-level monitor observations.

Previous work[5,23,24] has noted that OMI LUR modeling predicts a substantial high rural bias that has been greatly improved (from MB = 98.7% to 14.8% in 2019) with the inclusion of TROPOMI observations. Beyond this, the relationships between land use categories and surface-level NO_2 are often nonlinear (e.g., some cities with built up areas have strong public transportation infrastructure and others do not) and they will likely change in the future (e.g., as transportation transitions to electric vehicles in the US, road systems will be a weaker marker of NO_2).[59] Thus, the inclusion of refined satellite remote sensing in LUR modeling will allow for more dynamic models that can predict pollution levels across disparate geographies. TROPOMI is currently the most empirical way to surveil NO_2 globally, so we anticipate that a model more heavily based on TROPOMI might mitigate some of the issues from other models that assume NO_2 concentrations are in lockstep with land use. As satellite remote sensing observations of atmospheric composition become more accurate and finely resolved, future LUR models will likely become more capable at predicting surface-level NO_2 while simultaneously relying on fewer land-use predictor variables.

The inclusion of TROPOMI remote-sensing observations impacts LUR predictions by improving the predictive accuracy and supplanting the influence of land-use characteristic variables with remote-sensing observations. Specifically, the TROPOMI-LUR predicts monthly surface-level NO_2 in the CONUS that is well correlated (Adj. R^2 = 0.72) and minimally biased (MB = 14.2%) across 10,000 cross-validations for 2019−2022 compared to predictions from a global OMI-LUR (Adj. R^2 = 0.54 and MB = 49% in North America) for 2005−2019. Additionally, we find that the TROPOMI-LUR has a greater dependence on remote-sensing observations (29.1% reduction in R^2 when removed) than the OMI-LUR (6.2% globally; 15.2% max regional value). Our results suggest that finer-resolution remote-sensing observations of column NO_2 from TROPOMI improves the predictive capacity of LUR models and that TROPOMI-derived models rely less on land-use characteristics and depend more on remote-sensing observations. This implies that LUR models built using OMI observations may overemphasize the relationship between surface-level NO_2 and land-use characteristics as the latter have a greater influence on predictive accuracy. Additionally, the inclusion of observations from TROPOMI, instead of OMI, improves the ability of our LUR model to differentiate surface-level NO_2 concentrations across specific regions (see Figure S6 for an illustration in 2021). The inclusion of TROPOMI NO_2 in other statistical models would likely have similar impacts relative to OMI on the estimation of NO_2 concentrations, although we caution directly comparing model evaluation metrics across studies given the different spatiotemporal resolutions and coverage.

The TROPOMI-LUR predictions have similar accuracy and minimal biases across specific subgroups of monitors. For example, statistical performance was comparable throughout all

https://doi.org/10.1021/acsestair.4c00153
ACS EST Air 2025, 2, 187−200

four years indicating that the monthly TROPOMI-LUR predictions are equally accurate regardless of the year for which they are predicting and suggests that the modeling framework can be extended to future years without major concerns for changes in predictive accuracy if there are not major shifts in the patterns represented by the static predictor variables. One exceptional subgroup of monitors are the "urban near-road" monitors for which predictions are low biased. This low bias is likely at least partially attributable to the resolution of our TROPOMI-LUR model; the 1 × 1 km^2 resolution of our model is less likely to capture the fine-scale variability (∼50 m) in surface-level NO_2 that is observed by near-road monitors, which leads to a systematic underprediction of NO_2 at these locations. For a 1 × 1 km^2 LUR model, the performance at these near-road locations could only be improved at the detriment of nonroad locations, given that these monitors can occupy the same grid cell. This low bias could likely be addressed through the development of a fine-resolution (∼50 m) TROPOMI-LUR model in which sharper near-road gradients in NO_2 concentrations could be captured through the increased influence of predictor variables associated with fine-scale road systems.

The above findings and discussion should be considered together with potential uncertainties in our results and alongside assumptions that are made in our analysis. The applicability of LUR predictions is dependent on the representativeness of the monitor observations that the model is trained on; while we find that the TROPOMI-LUR predictions better capture patterns in EPA AQS observations at monitor locations than the OMI-LUR, we are unable to determine the efficacy of either LUR model for locations that are not well-represented in our training data set (e.g., rural mountain-west). This is especially notable as previous work[60] has found that TROPOMI may be unable to differentiate patterns in background NO_2. This poorer performance in the background could be attributed to sources of NO_2 away from the surface (i.e., lightning NO_x, advected wildfire plumes, and aircraft emissions) that are observed by TROPOMI but not picked up by ground-level monitors. Given the strong dependence of the TROPOMI-LUR on TROPOMI observations, the improvement found in predicted NO_2 compared to the OMI-LUR may be lessened in background areas in which we do not have observations. Another potential source of uncertainty in our analysis is the differences in resolution between the TROPOMI-LUR and OMI-LUR given that the TROPOMI-LUR developed in this work is much coarser (1 × 1 km^2) than the OMI-derived LUR (50 × 50 m^2). This resolution effect could also impact how predictor variables affect R^2 (Table 4) and perhaps lead to an underestimate of the influence of road systems. When developing the TROPOMI-LUR, we do not correct for a well-established high bias[27,61] in observations from chemiluminescent monitors for the purpose of comparison to the OMI-LUR which also did not incorporate this correction; additionally, many epidemiological studies have derived relationships between NO_2 and health effects that do not correct for this bias; however, we note that this could lead to an overestimate in predicted surface-level NO_2 by the TROPOMI-LUR.

While we find improved predictive accuracy in the TROPOMI-LUR model we note that there are still many applications for the inclusion of OMI observations. Given the greater temporal coverage of OMI (2005-present) there are more observations from OMI and subsequently more years of observations from which to build LUR models. This is especially applicable for multiyear retrospective epidemiological studies that require a long record of observations to determine statistical relationships between NO_2 exposure and health effects. For these types of studies, multidecadal products built by combining observations from different satellite instruments[62] could be used. Ultimately, the correlation between TROPOMI-LUR predictions and observations is much stronger than for the OMI-LUR indicating that variance in predicted NO_2 is captured with more accuracy when TROPOMI data is included.

The findings of this study could have significant impacts for applications in epidemiological and environmental justice studies. Given their stronger correlation and lower error when compared with observations, predictions generated by the TROPOMI-LUR demonstrate an increased capacity to differentiate NO_2 levels in different environments than the previous OMI-LUR that will have implications for multicity epidemiological studies. Comparative differences across different regions and cities are likely better captured in TROPOMI-LUR predictions which could have implications for both risk assessment and environmental justice analyses. For studies that focus on understanding the health effects associated with near-road exposure—within 50 m of a major highway—a negative bias (MB = −18.5%) in the TROPOMI-LUR should be considered and accounted for. The distribution of NO_2 within cities differs dramatically in the TROPOMI-LUR compared to the OMI-LUR; the former captures more diffuse gradients in NO_2 concentrations while the latter predicts sharper gradients associated with land-use characteristics. Given this, the NO_2 distributions predicted by the TROPOMI-LUR will be relatively higher for populations that are not directly adjacent to road systems but likely reduced for populations directly near roads compared to the OMI-LUR.

We find that the inclusion of finer-resolution oversampled remote-sensing observations from TROPOMI reduces the influence of land-use characteristics on predicting surface-level NO_2 and suggest that patterns in NO_2 distribution are less predictably related to land-use data than previously LUR models have estimated. With the availability of hourly surface-level NO_2 data at even finer spatial-resolution in the US from the NASA Tropospheric Emissions: Monitoring of Pollution (TEMPO) instrument, there is opportunity to further understand the distribution of surface-level NO_2 and how well it correlates with land-use characteristics. Considering the findings of this study, inclusion of finer resolved and more accurate satellite remote sensing observations of atmospheric composition leads to more accurate predictions of surface-level NO_2 that rely on fewer data inputs. As satellite remote-sensing capabilities continue to improve in the future, LURs that incorporate these data will likely be more straightforward, applicable to greater geographic extents, and more dynamic in the face of changing relationships between land-use categories and surface-level NO_2.

■ ASSOCIATED CONTENT

Data Availability Statement

All data are available in the main text or the Supporting Information except the surface NO_2 product that is accessible at: https://doi.org/10.5281/zenodo.14646033.

Supporting Information

The Supporting Information is available free of charge at https://pubs.acs.org/doi/10.1021/acsestair.4c00153.

https://doi.org/10.1021/acsestair.4c00153
ACS EST Air 2025, 2, 187−200

Two tables of summary statistics of the EPA AQS monitors at the monthly and annual time scales; Six figures including a methodological diagram, comparisons of model performance across different regions and seasons, and a comparison between TROPOMI and OMI model performance; Brief description of the statistical terms used throughout the manuscript (PDF)

AUTHOR INFORMATION

Corresponding Author

M. Omar Nawaz − *Department of Environmental and Occupational Health, Milken Institute School of Public Health, George Washington University, Washington D.C. 20037, United States;* orcid.org/0000-0001-7706-7287; Email: nawaz.muhammad@email.gwu.edu

Authors

Daniel L. Goldberg − *Department of Environmental and Occupational Health, Milken Institute School of Public Health, George Washington University, Washington D.C. 20037, United States*

Gaige H. Kerr − *Department of Environmental and Occupational Health, Milken Institute School of Public Health, George Washington University, Washington D.C. 20037, United States;* orcid.org/0000-0001-8869-0752

Susan C. Anenberg − *Department of Environmental and Occupational Health, Milken Institute School of Public Health, George Washington University, Washington D.C. 20037, United States*

Complete contact information is available at: https://pubs.acs.org/10.1021/acsestair.4c00153

Author Contributions

Conceptualization: MON, DLG, GK, SCA Methodology: MON, DLG, GK, SCA Investigation: MON Visualization: MON Supervision: DLG, SCA Writing—original draft: MON Writing—review and editing: MON, DLG, GK, SCA.

Funding

We gratefully acknowledge funding for this work from: NASA HAQAST (80NSSC21K0511), NASA ACMAP (80NSSC23K1002), NOAA (1305M323PNRMA0668), and NIH (138267-Z0725202).

Notes

The authors declare no competing financial interest.

ACKNOWLEDGMENTS

We gratefully acknowledge the computing resources provided on the High Performance Computing Cluster operated by Research Technology Services at the George Washington University.

REFERENCES

(1) McDuffie, E. E.; Martin, R. V.; Spadaro, J. V.; Burnett, R.; Smith, S. J.; O'Rourke, P.; Hammer, M. S.; van Donkelaar, A.; Bindle, L.; Shah, V.; Jaeglé, L.; Luo, G.; Yu, F.; Adeniran, J. A.; Lin, J.; Brauer, M. Source Sector and Fuel Contributions to Ambient PM2.5 and Attributable Mortality across Multiple Spatial Scales. *Nat. Commun.* **2021**, *12* (1), 3594.

(2) Costa, S.; Ferreira, J.; Silveira, C.; Costa, C.; Lopes, D.; Relvas, H.; Borrego, C.; Roebeling, P.; Miranda, A. I.; Paulo Teixeira, J. Integrating Health on Air Quality Assessment—Review Report on Health Risks of Two Major European Outdoor Air Pollutants: PM and NO2. *Journal of Toxicology and Environmental Health, Part B* **2014**, *17* (6), 307−340.

(3) Xue, T.; Tong, M.; Wang, M.; Yang, X.; Wang, Y.; Lin, H.; Liu, H.; Li, J.; Huang, C.; Meng, X.; Zheng, Y.; Tong, D.; Gong, J.; Zhang, S.; Zhu, T. Health Impacts of Long-Term NO2 Exposure and Inequalities among the Chinese Population from 2013 to 2020. *Environ. Sci. Technol.* **2023**, *57* (13), 5349−5357.

(4) Anenberg, S. C.; Henze, D. K.; Tinney, V.; Kinney, P. L.; Raich, W.; Fann, N.; Malley, C. S.; Roman, H.; Lamsal, L.; Duncan, B.; Martin, R. V.; van Donkelaar, A.; Brauer, M.; Doherty, R.; Jonson, J. E.; Davila, Y.; Sudo, K.; Kuylenstierna, J. C. I. Estimates of the Global Burden of Ambient PM2.5, Ozone, and NO2 on Asthma Incidence and Emergency Room Visits. *Environ. Health Perspect* **2018**, *126* (10), No. 107004.

(5) Anenberg, S. C.; Mohegh, A.; Goldberg, D. L.; Kerr, G. H.; Brauer, M.; Burkart, K.; Hystad, P.; Larkin, A.; Wozniak, S.; Lamsal, L. Long-Term Trends in Urban NO2 Concentrations and Associated Paediatric Asthma Incidence: Estimates from Global Datasets. *Lancet Planetary Health* **2022**, *6* (1), e49−e58.

(6) Achakulwisut, P.; Brauer, M.; Hystad, P.; Anenberg, S. C. Global, National, and Urban Burdens of Paediatric Asthma Incidence Attributable to Ambient NO2 Pollution: Estimates from Global Datasets. *Lancet Planetary Health* **2019**, *3* (4), e166−e178.

(7) Lange, K.; Richter, A.; Burrows, J. P. Variability of Nitrogen Oxide Emission Fluxes and Lifetimes Estimated from Sentinel-5P TROPOMI Observations. *Atmospheric Chemistry and Physics* **2022**, *22* (4), 2745−2767.

(8) Jacob, D. J. Heterogeneous Chemistry and Tropospheric Ozone. *Atmos. Environ.* **2000**, *34* (12), 2131−2159.

(9) Valin, L. C.; Russell, A. R.; Cohen, R. C. Variations of OH Radical in an Urban Plume Inferred from NO2 Column Measurements. *Geophys. Res. Lett.* **2013**, *40* (9), 1856−1860.

(10) Hoek, G.; Beelen, R.; de Hoogh, K.; Vienneau, D.; Gulliver, J.; Fischer, P.; Briggs, D. A Review of Land-Use Regression Models to Assess Spatial Variation of Outdoor Air Pollution. *Atmos. Environ.* **2008**, *42* (33), 7561−7578.

(11) Song, J.; Wang, Y.; Zhang, Q.; Qin, W.; Pan, R.; Yi, W.; Xu, Z.; Cheng, J.; Su, H. Premature Mortality Attributable to NO2 Exposure in Cities and the Role of Built Environment: A Global Analysis. *Sci. Total Environ.* **2023**, *866*, No. 161395.

(12) Mohegh, A.; Goldberg, D.; Achakulwisut, P.; Anenberg, S. C. Sensitivity of Estimated NO2-Attributable Pediatric Asthma Incidence to Grid Resolution and Urbanicity. *Environ. Res. Lett.* **2021**, *16* (1), No. 014019.

(13) Kerr, G. H.; van Donkelaar, A.; Martin, R. V.; Brauer, M.; Bukart, K.; Wozniak, S.; Goldberg, D. L.; Anenberg, S. C. Increasing Racial and Ethnic Disparities in Ambient Air Pollution-Attributable Morbidity and Mortality in the United States. *Environ. Health Perspect* **2024**, *132* (3), 37002.

(14) Kerr, G. H.; Goldberg, D. L.; Anenberg, S. C. COVID-19 Pandemic Reveals Persistent Disparities in Nitrogen Dioxide Pollution. *Proc. Natl. Acad. Sci. U. S. A.* **2021**, *118* (30), No. e2022409118.

(15) Goldberg, D. L.; Saide, P. E.; Lamsal, L. N.; de Foy, B.; Lu, Z.; Woo, J.-H.; Kim, Y.; Kim, J.; Gao, M.; Carmichael, G.; Streets, D. G. A Top-down Assessment Using OMI NO2 Suggests an Underestimate in the NOx Emissions Inventory in Seoul, South Korea, during KORUS-AQ. *Atmos. Chem. Phys.* **2019**, *19* (3), 1801−1818.

(16) Goldberg, D. L.; Anenberg, S. C.; Kerr, G. H.; Mohegh, A.; Lu, Z.; Streets, D. G. TROPOMI NO2 in the United States: A Detailed Look at the Annual Averages, Weekly Cycles, Effects of Temperature, and Correlation With Surface NO2 Concentrations. *Earth's Future* **2021**, *9* (4), No. e2020EF001665.

(17) Boersma, K. F.; Jacob, D. J.; Eskes, H. J.; Pinder, R. W.; Wang, J.; van der A, R. J. Intercomparison of SCIAMACHY and OMI Tropospheric NO2 Columns: Observing the Diurnal Evolution of Chemistry and Emissions from Space. *J. Geophys. Res.: Atmos.* **2008**, DOI: 10.1029/2007JD008816.

(18) Flores-Jiménez, D. E.; García-Cueto, O. R.; Santillán-Soto, N.; López-Velázquez, J. E.; Camargo-Bravo, A. Influence of Mixing Height and Atmospheric Stability Conditions on Correlation of NO2 Columns and Surface Concentrations in a Mexico-United States Border Region. *Atmospheric Science Letters* **2021**, *22* (6), No. e1024.
(19) Adams, T. J.; Geddes, J. A.; Lind, E. S. New Insights Into the Role of Atmospheric Transport and Mixing on Column and Surface Concentrations of NO2 at a Coastal Urban Site. *Journal of Geophysical Research: Atmospheres* **2023**, *128* (12), No. e2022JD038237.
(20) Liu, X.; Wang, Y.; Wasti, S.; Li, W.; Soleimanian, E.; Flynn, J.; Griggs, T.; Alvarez, S.; Sullivan, J. T.; Roots, M.; Twigg, L.; Gronoff, G.; Berkoff, T.; Walter, P.; Estes, M.; Hair, J. W.; Shingler, T.; Scarino, A. J.; Fenn, M.; Judd, L. Evaluating WRF-GC v2.0 Predictions of Boundary Layer Height and Vertical Ozone Profile during the 2021 TRACER-AQ Campaign in Houston, Texas. *Geoscientific Model Development* **2023**, *16* (18), 5493−5514.
(21) Cooper, M. J.; Martin, R. V.; McLinden, C. A.; Brook, J. R. Inferring Ground-Level Nitrogen Dioxide Concentrations at Fine Spatial Resolution Applied to the TROPOMI Satellite Instrument. *Environ. Res. Lett.* **2020**, *15* (10), No. 104013.
(22) Cooper, M. J.; Martin, R. V.; Hammer, M. S.; Levelt, P. F.; Veefkind, P.; Lamsal, L. N.; Krotkov, N. A.; Brook, J. R.; McLinden, C. A. Global Fine-Scale Changes in Ambient NO2 during COVID-19 Lockdowns. *Nature* **2022**, *601* (7893), 380−387.
(23) Larkin, A.; Geddes, J. A.; Martin, R. V.; Xiao, Q.; Liu, Y.; Marshall, J. D.; Brauer, M.; Hystad, P. Global Land Use Regression Model for Nitrogen Dioxide Air Pollution. *Environ. Sci. Technol.* **2017**, *51* (12), 6957−6964.
(24) Larkin, A.; Anenberg, S.; Goldberg, D. L.; Mohegh, A.; Brauer, M.; Hystad, P. A Global Spatial-Temporal Land Use Regression Model for Nitrogen Dioxide Air Pollution. *Front. Environ. Sci.* **2023**, DOI: 10.3389/fenvs.2023.1125979.
(25) European Space Agency. *Copernicus Sentinel-5P TROPOMI*, 2021. DOI: 10.5270/S5P-9bnp8q8.
(26) Palmer, P. I.; Jacob, D. J.; Chance, K.; Martin, R. V.; Spurr, R. J. D.; Kurosu, T. P.; Bey, I.; Yantosca, R.; Fiore, A.; Li, Q. Air Mass Factor Formulation for Spectroscopic Measurements from Satellites: Application to Formaldehyde Retrievals from the Global Ozone Monitoring Experiment. *Journal of Geophysical Research: Atmospheres* **2001**, *106* (D13), 14539−14550.
(27) Lamsal, L. N.; Martin, R. V.; van Donkelaar, A.; Steinbacher, M.; Celarier, E. A.; Bucsela, E.; Dunlea, E. J.; Pinto, J. P. Ground-Level Nitrogen Dioxide Concentrations Inferred from the Satellite-Borne Ozone Monitoring Instrument. *J. Geophys. Res.: Atmos.* **2008**, DOI: 10.1029/2007JD009235.
(28) Wu, S.; Huang, B.; Wang, J.; He, L.; Wang, Z.; Yan, Z.; Lao, X.; Zhang, F.; Liu, R.; Du, Z. Spatiotemporal Mapping and Assessment of Daily Ground NO2 Concentrations in China Using High-Resolution TROPOMI Retrievals. *Environ. Pollut.* **2021**, *273*, No. 116456.
(29) Kang, Y.; Choi, H.; Im, J.; Park, S.; Shin, M.; Song, C.-K.; Kim, S. Estimation of Surface-Level NO2 and O3 Concentrations Using TROPOMI Data and Machine Learning over East Asia. *Environ. Pollut.* **2021**, *288*, No. 117711.
(30) Long, S.; Wei, X.; Zhang, F.; Zhang, R.; Xu, J.; Wu, K.; Li, Q.; Li, W. Estimating Daily Ground-Level NO2 Concentrations over China Based on TROPOMI Observations and Machine Learning Approach. *Atmos. Environ.* **2022**, *289*, No. 119310.
(31) Dong, J.; Cai, X.; Tian, L.; Chen, F.; Xu, Q.; Li, T.; Chen, X. Satellite-Based Estimates of Daily NO2 Exposure in Urban Agglomerations of China and Application to Spatio-Temporal Characteristics of Hotspots. *Atmos. Environ.* **2023**, *293*, No. 119453.
(32) Yu, M.; Liu, Q. Deep Learning-Based Downscaling of Tropospheric Nitrogen Dioxide Using Ground-Level and Satellite Observations. *Science of The Total Environment* **2021**, *773*, No. 145145.
(33) Lee, H. J.; Liu, Y.; Chatfield, R. B. Neighborhood-Scale Ambient NO2 Concentrations Using TROPOMI NO2 Data: Applications for Spatially Comprehensive Exposure Assessment. *Science of The Total Environment* **2023**, *857*, No. 159342.
(34) Kim, M.; Brunner, D.; Kuhlmann, G. Importance of Satellite Observations for High-Resolution Mapping of near-Surface NO2 by Machine Learning. *Remote Sensing of Environment* **2021**, *264*, No. 112573.
(35) Virta, H.; Ialongo, I.; Szeląg, M.; Eskes, H. Estimating Surface-Level Nitrogen Dioxide Concentrations from Sentinel-5P/TROPOMI Observations in Finland. *Atmos. Environ.* **2023**, *312*, No. 119989.
(36) Pseftogkas, A.; Koukouli, M.-E.; Segers, A. *Comparison of S5P/TROPOMI Inferred NO2 Surface Concentrations with In Situ Measurements over Central Europe*. https://www.mdpi.com/2072-4292/14/19/4886 (accessed 2024−05−28).
(37) Chan, K. L.; Khorsandi, E.; Liu, S.; Baier, F.; Valks, P. Estimation of Surface NO2 Concentrations over Germany from TROPOMI Satellite Observations Using a Machine Learning Method. *Remote Sensing* **2021**, *13* (5), 969.
(38) Wang, Y.; Yuan, Q.; Li, T.; Zhu, L.; Zhang, L. Estimating Daily Full-Coverage near Surface O3, CO, and NO2 Concentrations at a High Spatial Resolution over China Based on S5P-TROPOMI and GEOS-FP. *ISPRS Journal of Photogrammetry and Remote Sensing* **2021**, *175*, 311−325.
(39) US EPA, O. *Near Road Monitoring*. https://www.epa.gov/amtic/near-road-monitoring (accessed 2024−04−25).
(40) Florczyk, A. J.; Ehrlich, D.; Freire, S.; Kemper, T.; Maffenini, L.; Melchiorri, M.; Pesaresi, M.; Politis, P.; Schiavina, M.; Sabo, F.; Zanchetta, L. *Global Human Settlement Layer*. European Commission. https://ghsl.jrc.ec.europa.eu/ghs_smod2019.php (accessed 2022−09−27).
(41) Malashock, D. A.; DeLang, M. N.; Becker, J. S.; Serre, M. L.; West, J. J.; Chang, K.-L.; Cooper, O. R.; Anenberg, S. C. Estimates of Ozone Concentrations and Attributable Mortality in Urban, Peri-Urban and Rural Areas Worldwide in 2019. *Environ. Res. Lett.* **2022**, *17* (5), No. 054023.
(42) Southerland, V. A; Brauer, M.; Mohegh, A.; Hammer, M. S; van Donkelaar, A.; Martin, R. V; Apte, J. S; Anenberg, S. C Global Urban Temporal Trends in Fine Particulate Matter (PM2·5) and Attributable Health Burdens: Estimates from Global Datasets. *Lancet Planetary Health* **2022**, *6* (2), e139−e146.
(43) C3S. *ERA5 hly Data on Single Levels from 1940 to Present*, 2018. DOI: 10.24381/CDS.ADBB2D47.
(44) Hersbach, H.; Bell, B.; Berrisford, P.; Hirahara, S.; Horányi, A.; Muñoz-Sabater, J.; Nicolas, J.; Peubey, C.; Radu, R.; Schepers, D.; Simmons, A.; Soci, C.; Abdalla, S.; Abellan, X.; Balsamo, G.; Bechtold, P.; Biavati, G.; Bidlot, J.; Bonavita, M.; De Chiara, G.; Dahlgren, P.; Dee, D.; Diamantakis, M.; Dragani, R.; Flemming, J.; Forbes, R.; Fuentes, M.; Geer, A.; Haimberger, L.; Healy, S.; Hogan, R. J.; Hólm, E.; Janisková, M.; Keeley, S.; Laloyaux, P.; Lopez, P.; Lupu, C.; Radnoti, G.; de Rosnay, P.; Rozum, I.; Vamborg, F.; Villaume, S.; Thépaut, J.-N. The ERA5 Global Reanalysis. *Quarterly Journal of the Royal Meteorological Society* **2020**, *146* (730), 1999−2049.
(45) Feng, M.; Sexton, J. O.; Channan, S.; Townshend, J. R. A Global, High-Resolution (30-m) Inland Water Body Dataset for 2000: First Results of a Topographic−Spectral Classification Algorithm. *International Journal of Digital Earth* **2016**, *9* (2), 113−133.
(46) Farr, T. G.; Rosen, P. A.; Caro, E.; Crippen, R.; Duren, R.; Hensley, S.; Kobrick, M.; Paller, M.; Rodriguez, E.; Roth, L.; Seal, D.; Shaffer, S.; Shimada, J.; Umland, J.; Werner, M.; Oskin, M.; Burbank, D.; Alsdorf, D. The Shuttle Radar Topography Mission. *Rev. Geophys.* **2007**, DOI: 10.1029/2005RG000183.
(47) Gong, P.; Li, X.; Wang, J.; Bai, Y.; Chen, B.; Hu, T.; Liu, X.; Xu, B.; Yang, J.; Zhang, W.; Zhou, Y. Annual Maps of Global Artificial Impervious Area (GAIA) between 1985 and 2018. *Remote Sensing of Environment* **2020**, *236*, No. 111510.
(48) Socioeconomic Data and Applications Center | SEDAC . https://sedac.ciesin.columbia.edu/ (accessed 2019−10−20).
(49) *OpenStreetMap*. OpenStreetMap. https://www.openstreetmap.org/copyright (accessed 2024−04−25).
(50) Ranstam, J.; Cook, J. A. LASSO Regression. *British Journal of Surgery* **2018**, *105* (10), 1348.

(51) Lamsal, L. N.; Duncan, B. N.; Yoshida, Y.; Krotkov, N. A.; Pickering, K. E.; Streets, D. G.; Lu, Z. U.S. NO2 Trends (2005−2013): EPA Air Quality System (AQS) Data versus Improved Observations from the Ozone Monitoring Instrument (OMI). *Atmos. Environ.* **2015**, *110*, 130−143.
(52) van der A, R. J.; Peters, D. H. M. U.; Eskes, H.; Boersma, K. F.; Van Roozendael, M.; De Smedt, I.; Kelder, H. M. Detection of the Trend and Seasonal Variation in Tropospheric NO2 over China. *J. Geophys. Res.: Atmos.* **2006**, DOI: 10.1029/2005JD006594.
(53) Campbell, P. C.; Tong, D.; Tang, Y.; Baker, B.; Lee, P.; Saylor, R.; Stein, A.; Ma, S.; Lamsal, L.; Qu, Z. Impacts of the COVID-19 Economic Slowdown on Ozone Pollution in the U.S. *Atmos. Environ.* **2021**, *264*, No. 118713.
(54) Copat, C.; Cristaldi, A.; Fiore, M.; Grasso, A.; Zuccarello, P.; Signorelli, S. S.; Conti, G. O.; Ferrante, M. The Role of Air Pollution (PM and NO2) in COVID-19 Spread and Lethality: A Systematic Review. *Environmental Research* **2020**, *191*, No. 110129.
(55) Liu, F.; Wang, M.; Zheng, M. Effects of COVID-19 Lockdown on Global Air Quality and Health. *Sci. Total Environ.* **2021**, *755*, No. 142533.
(56) Bechle, M. J.; Millet, D. B.; Marshall, J. D. Ambient NO2 Air Pollution and Public Schools in the United States: Relationships with Urbanicity, Race−Ethnicity, and Income. *Environ. Sci. Technol. Lett.* **2023**, *10*, 844.
(57) Mohegh, A.; Goldberg, D.; Achakulwisut, P.; Anenberg, S. C. Sensitivity of Estimated NO2-Attributable Pediatric Asthma Incidence to Grid Resolution and Urbanicity. *Environ. Res. Lett.* **2021**, *16* (1), No. 014019.
(58) Kerr, G. H.; Goldberg, D. L.; Knowland, K. E.; Keller, C. A.; Oladini, D.; Kheirbek, I.; Mahoney, L.; Lu, Z.; Anenberg, S. C. Diesel Passenger Vehicle Shares Influenced COVID-19 Changes in Urban Nitrogen Dioxide Pollution. *Environ. Res. Lett.* **2022**, *17* (7), No. 074010.
(59) Camilleri, S. F.; Montgomery, A.; Visa, M. A.; Schnell, J. L.; Adelman, Z. E.; Janssen, M.; Grubert, E. A.; Anenberg, S. C.; Horton, D. E. Air Quality, Health and Equity Implications of Electrifying Heavy-Duty Vehicles. *Nat. Sustain* **2023**, *6* (12), 1643−1653.
(60) Qu, Z.; Jacob, D. J.; Silvern, R. F.; Shah, V.; Campbell, P. C.; Valin, L. C.; Murray, L. T. US COVID-19 Shutdown Demonstrates Importance of Background NO2 in Inferring NOx Emissions From Satellite NO2 Observations. *Geophys. Res. Lett.* **2021**, *48* (10), No. e2021GL092783.
(61) Dunlea, E. J.; Herndon, S. C.; Nelson, D. D.; Volkamer, R. M.; San Martini, F.; Sheehy, P. M.; Zahniser, M. S.; Shorter, J. H.; Wormhoudt, J. C.; Lamb, B. K.; Allwine, E. J.; Gaffney, J. S.; Marley, N. A.; Grutter, M.; Marquez, C.; Blanco, S.; Cardenas, B.; Retama, A.; Ramos Villegas, C. R.; Kolb, C. E.; Molina, L. T.; Molina, M. J. Evaluation of Nitrogen Dioxide Chemiluminescence Monitors in a Polluted Urban Environment. *Atmospheric Chemistry and Physics* **2007**, *7* (10), 2691−2704.
(62) Lamsal, L. N.; Krotkov, N. A.; Marchenko, S. V.; Joiner, J.; Oman, L.; Vasilkov, A.; Fisher, B.; Qin, W.; Yang, E.-S.; Fasnacht, Z.; Choi, S.; Leonard, P.; Haffner, D. *TROPOMI/S5P NO2 Tropospheric, Stratospheric and Total Columns MINDS 1-Orbit L2 Swath 5.5 Km × 3.5 Km, NASA Goddard Space Flight Center, Goddard Earth Sciences Data and Information Services Center*, 2022.

https://doi.org/10.1021/acsestair.4c00153
ACS EST Air 2025, 2, 187−200